Optimization of microfluidic trap-based microsphere arrays

Article *in* Proceedings of SPIE - The International Society for Optical Engineering · March 2013

DOI: 10.1117/12.2006396

4 authors, including:

Xiaoxiao Xu
Washington University in St. Louis
20 PUBLICATIONS **422** CITATIONS
SEE PROFILE

Pinaki Sarder
University at Buffalo, The State University of New York
107 PUBLICATIONS **1,471** CITATIONS
SEE PROFILE

Zhenyu Li
George Washington University
89 PUBLICATIONS **1,584** CITATIONS
SEE PROFILE

Optimization of microfluidic trap-based microsphere arrays

Xiaoxiao Xu[a], Pinaki Sarder[b], Zhenyu Li[c], and Arye Nehorai[a]

[a]Preston M. Green Department of Electrical and Systems Engineering, Washington University in St. Louis, St. Louis, MO 63130, USA;
[b]Department of Electrical and Computer Engineering, The George Washington University, Washington, D.C., 20052, USA;
[c]The Mallinckrodt Institute of Radiology, Washington University School of Medicine in St. Louis, St. Louis, MO 63110, USA

ABSTRACT

We build a microfluidic trap-based microsphere array device. In the device, we design a novel geometric structure of the trap array and employ the hydrodynamic trapping mechanism to immobilize the microspheres. We develop a comprehensive and robust framework to optimize the values of the geometric parameters to maximize the microsphere arrays' packing density. We also simultaneously optimize multiple criteria, such as efficiently immobilizing a single microsphere in each trap, effectively eliminating fluidic errors such as channel clogging and multiple microspheres in a single trap, minimizing errors in subsequent imaging experiments, and easily recovering targets. Microsphere-trapping experiments have been performed using the optimized device and a device with un-optimized geometric parameters. These experiments demonstrate easy control of the transportation and manipulation of the microspheres in the optimized device. They also show that the optimized device greatly outperforms the un-optimized one.

Keywords: Microfluidics, Trap-based microsphere arrays, Optimization

1. INTRODUCTION

There has been a growing interest in developing lab-on-a-chip (LOC) or point of care (POC) medical diagnostic devices in recent years.[1–3] Microsphere arrays can detect diverse biological targets, such as DNAs, mRNAs, proteins, and cells in a single device, and thus have been proven to be a great platform for building LOC systems.[4] To fabricate the microsphere array device, the industrial standard methods are photolithography patterned insitu synthesis (such as Affymetrix),[5] and self-assembly of microspheres (such as Illumina).[6] However, photolithographic patterned microarrays are costly and complicated to implement.[5] Self-assembled microsphere arrays need specially fabricated substrates such as etched fiber optic bundles or silicon wafers, and thus they are also relatively expensive.[6] To eliminate these drawbacks of the standard methods, researchers recently have employed microfluidic techniques to implement a trap-based microsphere array system.[7,8] The microfluidics trap-based microsphere arrays have several advantages, such as having a fast reaction rate due to active flow and providing a gentle liquid environment for biological samples.

To improve the performance of the microfluidic trap-based microsphere array device as an independent and dedicated platform, a careful optimization of the device architecture is needed. Several criteria should be considered, including maximizing microspheres' packing density to make the device compact, efficiently immobilizing microspheres, effectively eliminating fluidic errors, minimizing errors introduced during the device's fabrication, and minimizing errors in the subsequent fluorescence imaging experiments.[9] Nevertheless, to date no studies have been reported about simultaneous optimization of these multiple criteria.

In this work, we develop a comprehensive and robust optimization framework on the device architecture. We first design for the microfluidic trap-based microsphere array device a novel trap array geometry (traps in inverted-trapezoid shapes) and employ a hydrodynamic trapping mechanism to immobilize the microspheres in the traps.

Further author information: (Send correspondence to A. Nehorai)
A.Nehorai: E-mail: nehorai@ese.wustl.edu, Telephone: 1 314 935 5565
X. Xu, P. Sarder, and Z. Li contributed equally to this work.

We then develop an analytical method to optimize the values of the trap's geometric parameters to maximize the microsphere arrays' packing density. In this optimization, we simultaneously satisfy also other criteria as mentioned above. We compute the optimized geometric parameters for a device capturing microspheres of radius 5 μm and further investigate the effects of the geometric parameters on the packing density. Microsphere-trapping experiments performed using the optimized device demonstrate the easy-control of the transportation, immobilization, and manipulation of microspheres in the trap arrays. We also fabricate another device with randomly selected values of the geometric parameters as the un-optimized device. Quantitative comparisons show that the optimized device greatly outperforms the un-optimized device. Particularly, the optimized device has a much higher packing density (1438 traps/mm^2) than that of the un-optimized one (762 traps/mm^2). Moreover, the optimized device has a higher microsphere trapping efficiency (a single microsphere in a trap) than the un-optimized one. For the former more than 99% of the traps are found to be filled with a single microsphere, whereas for the latter the percentage is 58%.

This paper is organized as follows. In Section 2, we describe the design of our device and the optimization framework. In Section 3, we compute the optimized geometric parameters for a device capturing microspheres of radius 5 μm and investigate the effects of these parameters on the packing density. In Section 4, we compare the performance of the optimized device and the un-optimized device through microsphere-trapping experiments. We also discuss the comparison between our device and self assembled three-dimensional (3D) microarrays. Section 5 concludes the paper.

2. OPTIMIZATION OF MICROFLUIDIC TRAP-BASED MICROSPHERE ARRAYS

We first briefly describe the structure of our trap-based microsphere arrays and their hydrodynamic trapping mechanism. We then present the geometry of a single trap and formulate the optimization problem for this geometry.

2.1 Structure of the microfluidic trap-based microsphere arrays

In Fig. 1, we present a schematic of the top view of the microfluidic channels with hydrodynamic trap arrays. The traps in the arrays are made of polydimethylsiloxane (PDMS). Each trap is made of inverted-trapezoid grooves. The microfluidic channels are connected with each other by a common inlet and outlet, as shown in Fig. 1a. To fill the traps, a liquid, such as phosphate buffered saline (PBS), containing the microspheres with specific receptors flows through the channels. The microspheres are immobilized by the traps during the process. To avoid cross contamination, in the intermissions of the microspheres' loading operation, the residual spheres are washed out using buffer solution.

In our design, each row of the traps is offset horizontally with respect to the one above it (Fig. 1a). This offset ensures the microspheres not trapped by the first row can easily be captured by the next row of traps. The separations between adjacent traps and rows are optimized to ensure minimal channel clogging*. Such separations also eliminate the possibility of two microspheres arriving at a trap simultaneously and intending to fill in the same trap.

Next we will present the proposed trap geometry, and then discuss the formulation of the optimization for this geometry, including the objective function and constraints.

2.2 Trap geometry and optimization

The proposed device employs fluidic resistance engineering to perform hydrodynamic trapping of microspheres.[8, 11, 12] Fig. 1b shows a schematic of the possible flow paths of a microsphere, which explains this hydrodynamic trapping mechanism. In this figure, path P_1 (pink line) is the *trapping* path and path P_2 (orange line) is the *bypassing* path. Here we define *trapping* as a microsphere flowing into the trap, and we define *bypassing* as the flow of subsequent microspheres through the channels next to the trap. We note that this scheme for a single trap is applicable for all the traps.

*Channel clogging refers to obstruction in a channel region that restricts the flow of microspheres. As a result, unwanted microspheres aggregate in that region.[10]

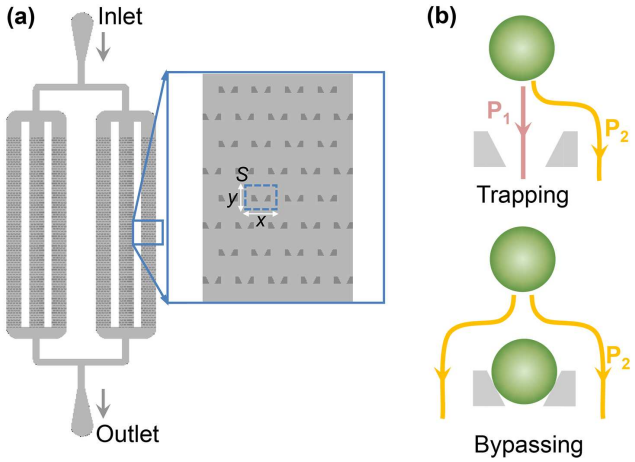

Figure 1. Schematic of the microfluidic trap-based microsphere arrays. (a) Layout: Microfluidic channels are connected by a common inlet and a common outlet. Liquid solution carrying the microspheres flows from the inlet and through the chamber. Microspheres are trapped by the hydrodynamic trap arrays during the process. In a zoomed-in view of trap arrays in a microfluidic channel, the blue dashed square shows a single trap for capturing one microsphere. The area of the single trap and its surroundings is denoted as S, whose length and width are defined by x and y. (b) Hydrodynamic trapping mechanism: The top figure shows how an empty trap automatically captures a single microsphere, because the corresponding path P_1 is designed to have a lower flow resistance than path P_2. This mechanism is denoted as *trapping*. When the trap through path P_1 is filled, the flow resistance of path P_1 increases to be much larger than that in path P_2. Thus, subsequent microspheres flow through path P_2. This mechanism is denoted as *bypassing*.

To trap the microspheres as shown in Fig. 1b, the trap array geometry should be designed so that the *trapping* path P_1 for an empty trap has a lower flow resistance than the *bypassing* path P_2. Then during the loading process, a microsphere in the fluid is most likely to move into an empty trap through P_1 (Fig. 1b top). However, once the trap through P_1 is loaded by a microsphere, the flow resistance in P_1 dramatically increases and is much larger than that in P_2, and thus subsequent microspheres divert to path P_2 and bypass the filled trap (Fig. 1b bottom).

Based on the hydrodynamic trapping mechanism, we have designed our trap array geometry to immobilize the microspheres and ensure a single microsphere in each trap. We have optimized this geometry to increase the microspheres' packing density and simultaneously satisfied other design criteria, such as eliminating channel clogging,[10] avoiding multiple microspheres trapping at one trap location, satisfying the trap array device's microfabrication tolerance and feasibility,[13] and achieving the optimal distance d_{opt} between microspheres obtained in the statistical design to minimize image analysis error.[9]

Fig. 2 shows a schematic diagram of the trap geometry with the corresponding geometric parameters. We define the radius of the microsphere as r; the height of the groove (i.e., height of the channel) as h; the length and the upper width of the groove walls as l and t, respectively; the trapezoid angle of the trap as α; and the upper and the bottom widths of the trap opening as u and b, respectively. We also define the width of the channel as g, the distance between two microspheres in the same row as d, and the minimal distance between a trap and a microsphere filled in a consecutive row as v. To eliminate the units of these parameters, we normalize them by dividing by the groove height h. We use below the sign $\tilde{}$ to represent the resulting parameters; e.g., $\tilde{r}$ represents the normalized r. Furthermore, we define the area of a single trap and its surroundings as S, whose length and width are x and y, respectively (see the white dashed square in Fig. 1a; inset ***b***). We finally define the packing density of the arrays as ρ.

2.2.1 Optimization objective function

Our optimization objective is to maximize ρ of the microsphere arrays. This is equivalent to minimizing the area S of each trap and its surroundings, as seen in Figs. 1 and 2. From these figures,

$$x = u + 2t + g, \quad y = g + l, \quad S = xy. \tag{1}$$

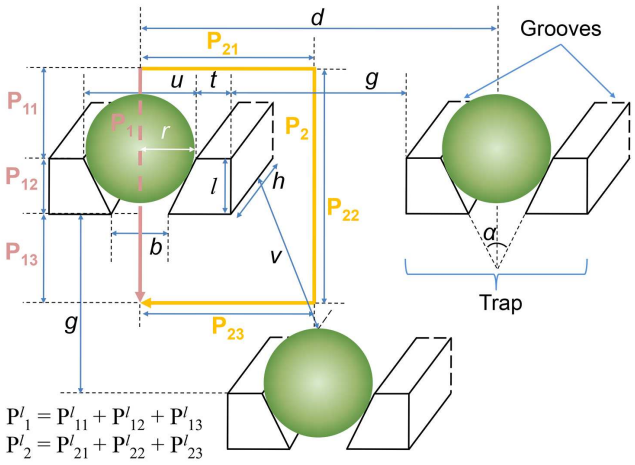

Figure 2. Schematic diagram of the trap array geometry. Three adjacent traps are presented here, with the first two traps in the same row and the third trap in a subsequent row. Each trap is made of inverted-trapezoid grooves. Two flow paths, the *trapping* path (pink line) and the *bypassing* path (orange line), of a microsphere encountering the first trap are shown here. The microsphere follows the *trapping* path when it encounters smaller flow resistance in this path than in the *bypassing* path; conversely, it follows the *bypassing* path. The *trapping* path contains the sub-paths P_{11}, P_{12}, and P_{13}, and the *bypassing* path contains the sub-paths P_{21}, P_{22}, P_{23}, P_{24}, and P_{25}.

Thus the optimization objective is $\rho = 1/S$, where S is to be minimized with respect to the trap array geometric parameters $\boldsymbol{\delta} = [r, h, l, u, b, t, g, d, v]^T$. For simplicity, the values of r and h are fixed in $\boldsymbol{\delta}$, and the other parameters are denoted as the optimization parameters. Therefore, the optimization objective is

$$\rho_{\mathrm{opt}} = 1/S_{\mathrm{opt}}, \ \mathrm{with} S_{\mathrm{opt}} = h^2 \cdot \min_{\boldsymbol{\delta}} (\tilde{g} + \tilde{l}) \cdot (\tilde{u} + 2\tilde{t} + \tilde{g}). \tag{2}$$

2.2.2 Optimization constraints

We formulate the optimization constraints to satisfy the multiple criteria we have proposed, i.e., the desired hydrodynamic trapping, a high microsphere trapping efficiency, minimal fluidic errors, a feasible device fabrication, and minimal errors in imaging experiments.

Constraint 1: We first formalize the constraint for the desired hydrodynamic trapping. According to this mechanism, for an empty trap, we require a smaller flow resistance in path P_1 (pink line in Fig. 2) than that in path P_2 (orange line). This in turn requires the volumetric flow rate Q_1 along the path P_1 be higher than the rate Q_2 along the path P_2,[11,12] and thus the volumetric flow rate[†]ratio $Q_1/Q_2 > 1$. Volumetric flow rates Q_1 and Q_2 are related to the pressure drops along the paths P_1 (ΔP_1) and P_2 (ΔP_2), respectively.[11,12] Therefore, we first derive ΔP_1 and ΔP_2.

The pressure drop ΔP in a rectangular microchannel is derived by Darcy-Weisbach equation and continuity and momentum equations for the Hagen-Poiseuille flow.[8,15] We assume fully established laminar flow inside the trapping area here, which can be achieved by fabricating the trapping area far away from the fluid entrance. The expression of ΔP is expressed as

$$\Delta P = \frac{f(\beta)\mu Q C^2 L}{32 A^3}, \tag{3}$$

where μ denotes the fluid viscosity, L denotes the length of the channel, Q denotes the volumetric flow rate, and A and C denote the channel's cross-sectional area and perimeter. The function $f(\beta)$ is a known polynomial of the aspect ratio β,[14]

$$f(\beta) = 96(1 - 1.3553\beta + 1.9467\beta^2 - 1.7012\beta^3 + 0.9564\beta^4 - 0.2537\beta^5),$$

[†]Volumetric flow rate defines the volume of fluid that passes through a given surface per unit time.[14]

where β is the ratio of the height and width of the rectangular channel, such that $0 \leq \beta \leq 1$.

For our trap array geometry in Fig. 2, we compute ΔP_1 and ΔP_2 as below.

• ΔP_1 (pink line in Fig. 2): Path P_1 contains the sub-paths P_{11} (above the trap), P_{12} (through the trap), and P_{13} (below the trap). The length of P_{12} is $\mathrm{P}_{12}^l = l$. The width of P_{12} changes continuously from the top width u to the bottom width b of the trap opening, both of which are several μm long. Meanwhile, the widths of P_{11} and P_{13} equal the length of the whole horizontal channel, which is more than 1×10^3 μm long. In other words, the widths of P_{11} and P_{13} are much greater than that of P_{12}, so that the pressure drops along P_{11} and P_{13} are negligible. Therefore, most of the pressure drop in P_1 happens along P_{12}.[14]

From Eqn. (3) and Fig. 2, we have ΔP_1 as

$$\Delta P_1 = \int_0^l \frac{f(\beta)\mu Q_1 C^2}{32A^3}\,\mathrm{d}l'. \tag{4}$$

where, $A = wh$, $C = 2(w+h)$, $\beta = w/h$, with w as the width of P_{12}. For the sub-path P_{12} through the trap, at any moment the microsphere is flowing in a piece-wise rectangular channel of infinitesimally small width $\mathrm{d}w$, with the infinitesimal metric changes with the length l of the triangular shape inside the trap. We thus substitute w with l while deriving the pressure drop along P_{12}. Therefore, we substitute $w = \frac{(b-u)}{l} \cdot l' + u$, $\tilde{w} = w/h$, and $\tilde{l}' = l'/h$ into Eqn. (4)

$$\Delta P_1 = \int_0^{\tilde{l}} \frac{f(\tilde{w})\mu Q_1 (\tilde{w}+1)^2}{8\tilde{w}^3 h^3}\,\mathrm{d}\tilde{l}'. \tag{5}$$

• ΔP_2 (orange line in Fig. 2): Path P_2 has the same start and end points as path P_1. It contains the sub-paths P_{21} (above the trap), P_{22} (above the separation between the traps), P_{23} (through the separation between the traps), P_{24} (below the separation between the traps), and P_{25} (below the trap). Likewise, the widths of P_{22} and P_{24} equal the length of the whole horizontal channel, which are so large that the pressure drops along them are negligible. Most of the pressure drops occur along the sub-paths P_{21}, P_{23}, and P_{25}, which have the same width g. The length of P_2^l becomes $\mathrm{P}_2^l = \mathrm{P}_{21}^l + \mathrm{P}_{23}^l + \mathrm{P}_{25}^l = u + 2t + g + l$. Therefore, we substitute $A = gh$ and $C = 2(g+h)$ into Eqn. (3), we have ΔP_2 as

$$\Delta P_2 = \frac{f(\bar{\tilde{g}})\mu Q_2 (\tilde{g}+1)^2 \tilde{\mathrm{P}}_2^l}{8\tilde{g}^3 h^3}, \tag{6}$$

where, $\tilde{\mathrm{P}}_2^l = \mathrm{P}_2^l/h$, $\bar{\tilde{g}} = \tilde{g}$ if $\tilde{g} \leq 1$, otherwise, $\bar{\tilde{g}} = \tilde{g}^{-1}$.

• We equate ΔP_1 and ΔP_2 and obtain the expression of Q_1/Q_2. To satisfy hydrodynamic trapping, we require $Q_1/Q_2 > 1$. Therefore, *Constraint 1* is $\mathbf{C}_1 = \{G(\boldsymbol{\delta}) < 0\}$, where

$$G(\boldsymbol{\delta}) = \int_0^{\tilde{l}} \frac{f(\tilde{w})(\tilde{w}+1)^2}{w^3}\,\mathrm{d}\tilde{l}' - \frac{f(\bar{\tilde{g}})(\tilde{g}+1)^2 \tilde{\mathrm{P}}_2^l}{\tilde{g}^3}. \tag{7}$$

Constraint 2: To ensure that a single microsphere is trapped in a single trap and to avoid multiple microspheres in a trap, we require u and l to be smaller than the sum of two microspheres' diameters ($\tilde{u} < 4\tilde{r}$ and $\tilde{l} < 4\tilde{r}$). We also require b to be smaller than the microsphere's diameter ($\tilde{b} < 2\tilde{r}$). To avoid the possibilities that fabrication variations cause these parameters fail this constraint, we employ 2 μm safety margins in the constraint.[16] Therefore, *Constraint 2* is $\mathbf{C}_2 = \{\tilde{b} \leq 2\tilde{r} - 2/h,\ \tilde{u} \leq 4\tilde{r} - 2/h,\ \tilde{l} \leq 4\tilde{r} - 2/h\}$.

Constraint 3: To ensure stable trapping of the microspheres, i.e., a microsphere is retained in a trap and is not swept away by the transient flow, we require the trapezoid angle $\alpha = 2\arctan\left(\frac{0.5(\tilde{u}-\tilde{b})}{\tilde{l}}\right)$ to be greater than 5°. We also require l to be greater than the microsphere's radius ($l > r$). Therefore, *Constraint 3* is $\mathbf{C}_3 = \{-\alpha \leq -5°,\ -\tilde{l} \leq -\tilde{r}\}$.

Constraint 4: To avoid channel clogging, we require $\tilde{g} < 4\tilde{r}$ to avoid multiple microspheres flowing simultaneously through the channel. We also require only one microsphere to flow through the channel during the *bypassing*

process ($\tilde{g} > 2\tilde{r}$). Allowing for fabrication variations, we again use 2 μm margins. Therefore, *Constraint 4* is $2\tilde{r} + 2/h < \tilde{g} < 4\tilde{r} - 2/h$.

We also require v to be greater than the microsphere's diameter, i.e., $\tilde{v} > 2\tilde{r}$, where $\tilde{v}^2 = (\tilde{g} - \sqrt[2]{\max(0, \tilde{r}^2 - (0.5\tilde{u})^2)} - \tilde{r})^2 + (0.5\tilde{g})^2$. Considering fabrication variations, we change the requirement to $\tilde{v} > 2\tilde{r} + 2/h$. Therefore, *Constraint 4* is $\mathbf{C}_4 = \{\tilde{g} \leq 4\tilde{r} - 2/h, -\tilde{g} \leq -2\tilde{r} - 2/h, -\tilde{v} \leq -2\tilde{r} - 2/h\}$.

Constraint 5: Considering the feasibility in chip fabrication, we require the possible aspect ratios (the ratio of transverse dimensions to height, for example, t/h, i.e., $\tilde{t}$) of the geometric parameters in the device to be in the range of $[0.4, 2.5]$. Aspect ratios that are too small cause difficulty in fabricating the features using soft lithography, while aspect ratios of the channels that are too large cause the traps easily collapse. Therefore, *Constraint 5* is $\mathbf{C}_5 = \{\tilde{l}, \tilde{g}, \tilde{b}, \tilde{u}, \tilde{t} \leq 2.5, -\tilde{l}, -\tilde{g}, -\tilde{b}, -\tilde{u}, -\tilde{t} \leq -0.4\}$.

Constraint 6: To minimize the error in imaging the targets captured by the microspheres, we require the distance $d = u + 2t + g$ between the centers of two immobilized microspheres to be greater than the minimal distance d_{opt} computed in our earlier publication.[9] Therefore, *Constraint 6* is $\mathbf{C}_6 = \{-\tilde{d} \leq -\frac{d_{\text{opt}}}{h}\}$.

To summarize, the optimization problem is

$$\boxed{\rho_{\text{opt}} = 1/S_{\text{opt}},\ \text{with} S_{\text{opt}} = h^2 \cdot \min_{\boldsymbol{\delta}} (\tilde{g} + \tilde{l}) \cdot (\tilde{u} + 2\tilde{t} + \tilde{g}),} \tag{8}$$

where $\boldsymbol{\delta} \in \{\mathbf{C}_1 \bigcap \mathbf{C}_2 \bigcap \mathbf{C}_3 \bigcap \mathbf{C}_4 \bigcap \mathbf{C}_5 \bigcap \mathbf{C}_6\}$.

To solve Eqn. (8), we used the interior-point optimization algorithm,[17] and the grid-search method[18] on the feasible parameter space defined by $\boldsymbol{\delta}$.

3. NUMERICAL EXAMPLES

In the numerical example, we compute the optimal trap array geometry for immobilizing microspheres of radius $r = 5$ μm. We also study the effects of the optimization geometric parameters in $\boldsymbol{\delta}$ on the packing density ρ.

We first assign the fixed parameter h as 13 μm, for microspheres of radius 5 μm. Though h does not affect the packing density of the device, it should be larger than the microsphere's diameter to avoid the microsphere flowing out of the channel. It also should be shallow enough to avoid one microsphere flowing on top of another microsphere so that the two arrive at the trap simultaneously. Based on experimental testing results, we choose $h = 2.6r$. Moreover, the minimal distance d_{opt} to minimize the imaging error for microspheres of radius 5 μm is 20 μm.[9]

We then obtain the optimal values of the optimization parameters in $\boldsymbol{\delta}$. As stated, we use the interior-point algorithm and the grid-search method to solve Eqn. (8). The two optimization methods give almost identical results for the optimization parameters l, u, b, t, and g (Table 1). We note that the parameters d and v in $\boldsymbol{\delta}$ are not listed as they are functions of the other parameters. The S_{opt} computed from the interior-point method and the grid-search method are 690.61 mm^2 and 686.39 mm^2, respectively, with corresponding ρ_{opt} of 1448 traps/mm^2 and 1456 traps/mm^2.

To evaluate the effects of the optimization geometric parameters and compare the sensitivities of ρ in response to their changes, we plot ρ as individual functions of l, u, b, t, and g (Fig. 3). In each sub-plot of a specific parameter, we use this parameter's feasible range determined by the optimization constraints (Eqn. (8)) as the range of the x-axis, and we set the other four parameters are at their optimal values. For example, in Fig. 3a, l

Table 1. Fixed and optimization geometric parameters for the microfluidic trap-based microsphere array

Fixed Values (μm)	r	h			
	5	13			
Optimized Values (μm)	l_{opt}	u_{opt}	b_{opt}	t_{opt}	g_{opt}
Interior-point method	5.210	10.001	6.915	5.205	14.546
Grid-search method	5.200	10.020	6.900	5.200	14.600

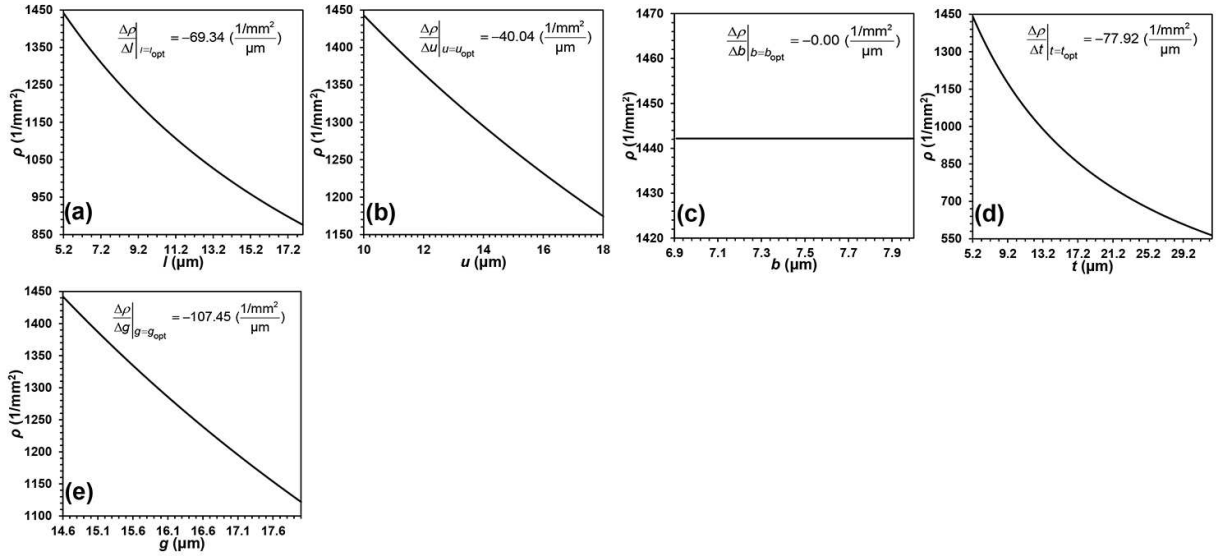

Figure 3. Effects of the optimization geometric parameters of (a) l, (b) u, (c) b, (d) t, and (e) g, on the packing density ρ of the microfluidic trap-based microsphere arrays. These parameters are plotted in their feasible ranges by the optimization constraints. The first derivatives of ρ with respective to l, u, b, t, and g are computed at these parameters' optimal values obtained from the grid-search method.

is feasible in the range [5.2 μm, 18 μm], $u = u_{\text{opt}}$ (10.02 μm), $b = b_{\text{opt}}$ (6.9 μm), $t = t_{\text{opt}}$ (5.2 μm), and $g = g_{\text{opt}}$ (14.6 μm). Among the five parameters, g has the greatest effect on ρ (Fig. 3e). Explicitly, ρ has the largest first derivative of with respective to g, so that a slight increase of g away from its optimal value $g_{\text{opt}} = 14.6$ μm leads to a large decrease of ρ. Contrarily, ρ is less sensitive to the changes of l, u, and t, so they are less influential on ρ (Fig. 3a, 3c, and 3d, respectively). ρ is independent of b (Fig. 3b). We also see from Fig. 3 that the feasible ranges of the five parameters are large enough to tolerate fabrication errors. The analysis of these geometric parameters reflects their relative significance and guides us in controlling the precision of these parameters in fabrication.

4. EXPERIMENTAL RESULTS AND DISCUSSION

To evaluate the optimization results, we fabricated ten microfluidic trap-based microsphere array devices with the optimized geometric parameters obtained from the numerical example. To compare the performance of the optimized devices, we also fabricated another ten devices, the geometric parameters of which were randomly selected, satisfying only the flow resistance constraint to ensure hydrodynamic trapping (*Constraint 1*). For convenient reference, we denote these ten devices as un-optimized devices, though their parameters' values may not satisfy the other proposed constraints. The geometric parameters of the optimized and un-optimized devices are listed in Table 2. Allowing for fabrication feasibility, we constrained the precision of the parameters to 0.1 μm. We performed a number of microsphere-trapping experiments using each set. Details are given below.

4.1 Device fabrication and operation

Microfluidic trap array devices were fabricated by using standard soft lithography techniques.[19] The devices were made of PDMS, a widely used material in microfluidics and micro-optics. We first fabricated a patterned photoresist SU8 mold on a silicon wafer using photolithography. We then poured PDMS prepolymer (RTV615,

Table 2. Geometric parameters of the optimized and un-optimized microfluidic trap-based microsphere arrays

Values (μm)	h	l	u	b	t	g
Optimized device	13	5.2	10.1	6.9	5.2	14.6
Un-optimized device	13	14.6	27.5	5.0	17.5	12.5

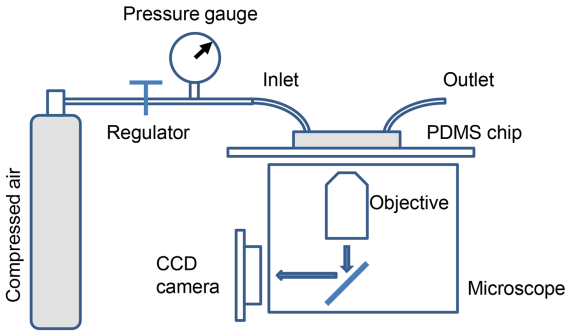

Figure 4. Schematic diagram of the experimental set-up.

1:10 ratio) onto the mold to be degassed in a vacuum chamber. The prepolymer was partially cured in a 60°C oven for 45 minutes. The 45 min curing time was found to be optimal as: shorter curing time led to collapsed structures in the final device, and longer curing time made the release of PDMS from the mold difficult. We peeled the partially cured PDMS off from the mold, and used a biopsy punch to punch the liquid inlet and outlet ports through the whole layer of the PDMS. We finally bonded the PDMS layer to a standard glass slide by oxygen plasma treatment. The master SU8 molds could be reused many times, and thus they reduce the fabrication cost and time.

The schematic diagram of the experimental set-up is shown in Fig. 4. We mounted the PDMS microfluidic device on an inverted microscope (Olympus IX71, San Jose, CA) equipped with an iXon+ EMCCD camera (Andor, South Windsor, CT). We then prepared a solution of 10 μm polystyrene microspheres (Bangs Lab, Fishers, IN) in 1X PBS buffer with 0.05% Tween-20 (Sigma Aldrich, St. Louis, MO) at a concentration of 10^5/mL. We loaded the microsphere solution into a 22 gauge Tygon tubing (Cole Parmer, Vernon Hills, IL). One end of the tubing was connected to the device input port via a stainless steel tube and the other end was connected to a pressure source controlled by a pressure regulator with a resolution of 0.4 psi. We pushed the microsphere solution into the device by applying 1-2 psi pressure to the Tygon tubing. We finally captured snapshots and videos of the microsphere trapping process, using the EMCCD camera. In the experiments, both optimized and un-optimized devices were tested under the same operation conditions, including driving pressure, microsphere concentration, and microsphere solution viscosity, etc.

4.2 Results

The results of the microsphere-trapping experiments of the optimized and un-optimized devices are presented here. Recall that the optimization objective is to maximize the packing density ρ of the trap arrays, ensure a single microsphere in each trap, and avoid multiple microspheres in each trap and channel clogging. For performance comparison, besides ρ, we define four experimental measurements as follows:

- *single*, the fraction of traps that immobilizes a single microsphere;
- *multiple*, the fraction of traps that immobilizes multiple microspheres;
- *empty*, the fraction of traps that do not immobilize any microspheres;
- *clogged*, the fraction of clogged channels.

We highlighted the illustrative examples of the above measurements in Fig. 5c in circles. Intuitively, we want for an optimized device large values for ρ and *single* but small values for *multiple*, *empty*, and *clogged*.

We compute the areas of each trap for the optimized device and the un-optimized device as 694.98 μm^2 and 1312.5 μm^2. Therefore, the packing densities ρ of the two devices are 1438 traps/mm^2 and 762 traps/mm^2, respectively. In other words, the optimized one improves the packing density by a factor of two from the un-optimized device.

Fig. 5 presents snapshots of one microsphere-trapping experiment at three critical time points: the start (Fig. 5a), middle (Fig. 5b), and end (Fig. 5c). Compared with the un-optimized device, the optimized one is remarkably more neat and compact in the layout of the trapped microspheres (larger *single*; smaller *multiple*, *empty*, and *clogged*). Though the time to completely fill up the traps is slightly longer for the optimized device

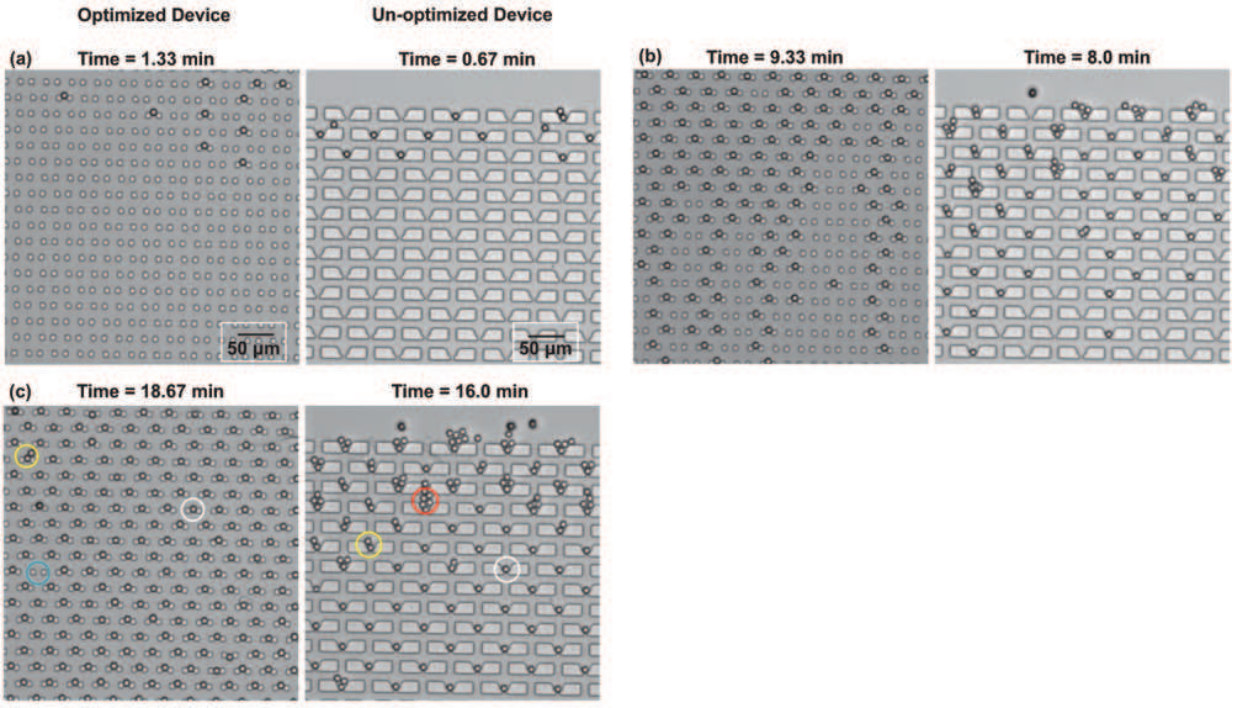

Figure 5. Time-lapse high-speed camera snapshots of one microsphere-trapping experiment of an optimized device (left) and an un-optimized device (right), at (a) the start time point, (b) the middle time point, and (c) the end time point. Illustrative examples of experimental measurements: *single* (white circle), *multiple* (yellow circle), *empty* (blue circle), and *clogged* (red circle) are highlighted in (c). Note that *clogged* is not found in the optimized device, nether is *empty* in the un-optimized device.

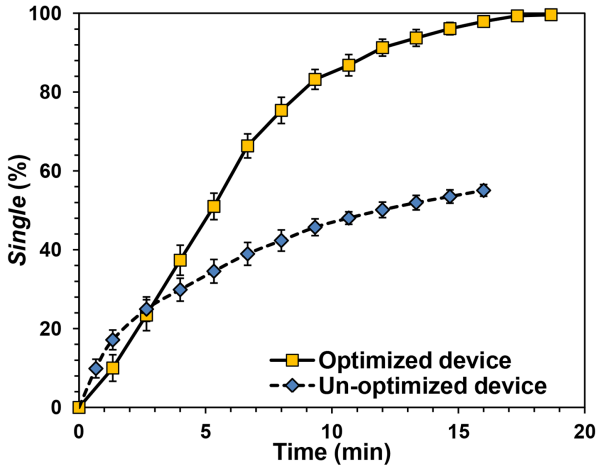

Figure 6. Time-lapse plots of the *single* values of the optimized device and the un-optimized device, with each has five replicate trapping experiments. The average experiment times taken to fill all the traps for the optimized device and the un-optimized device are 18.67 min and 16.0 min, respectively. Error bars indicate the standard deviations.

(18.67 min) than the un-optimized one(16 min), the optimized device traps many more microspheres, virtually all of them *single*.

Fig. 6 plots the values of *single* of the optimized and un-optimized devices as a function of microsphere-trapping experiment time, with five replicate experiments on each device. The *single* value of the optimized device increases sharply until 14 min, when over 90% of the traps are occupied with a single microsphere. After

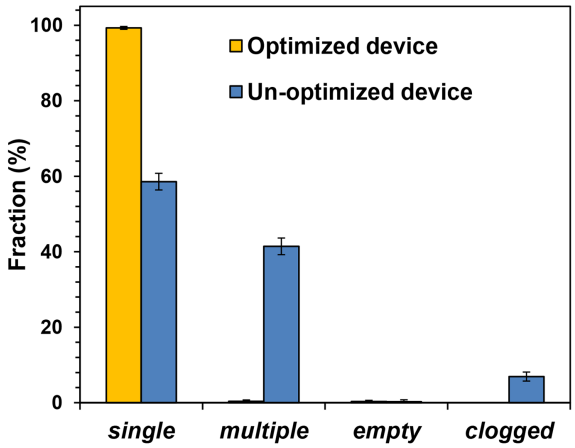

Figure 7. Experimental measurements for the optimized devices and un-optimized devices at the end of the experiments. The reported values are averaged results from ten devices, with error bars indicating the standard deviations of the results on the ten devices.

this time point, because the still-available traps may be relatively less accessible, the increase of *single* slows down. At the end, *single* of the optimized device achieves more than 99%. In contrast, the *single* value of the un-optimized device experiences a slow and concave increase from the beginning and is around 58% at the end. This figure confirms that the optimized device is more efficient and accurate in trapping a single microsphere in each trap.

Fig. 7 shows the final experimental results of the optimized and un-optimized devices. Explicitly, the *single*, *multiple*, *empty*, and *clogged* of ten optimized and ten un-optimized devices at the end of the experiments are plotted. In Fig. 7, the standard deviations of these measurements for both devices are small, suggesting that the trapping results are highly reproducible. The values of *empty* are close to 0% for both devices, indicating that almost no traps remain empty at the end. As long as there are paths for the microspheres to reach the empty traps, these traps will be eventually filled. Nevertheless, filling the empty traps may in turn result in more microspheres trapped at a single trap or clog the channels. As we have observed from Figs. 5c and 7, the optimized device avoids such risk. In other words, in the optimized device, most of the microspheres, if not immobilized in the empty traps, will pass by the channels directly. Therefore, in the optimized device, *single* is dominant (99.29%) and the undesired *multiple* and *clogged* are negligible (0.38% and 0%, respectively). On the contrary, in the un-optimized device the risk of multiple-trapping and channel clogging is dramatic (Fig. 5c). Therefore, compared to the optimized device, *single* of the un-optimized device is much lower (58.57%), and its *multiple* and *clogged* are much higher (41.43% and 6.93%, respectively). In summary, Fig. 7 confirms the outstanding performance based on the optimization with highly reproducible experimental results.

The microsphere-trapping experiments, with highly reproducible results, successfully demonstrate the advantages of the optimized device over the un-optimized device. The optimized device remarkably improves the packing density and the trapping efficiency, and effectively reduces the undesirable behaviors (multiple trapping and channel clogging) in the experiments.

The optimization framework for building the optimal structure of the microfluidic trap-based microsphere arrays is comprehensive. The hydrodynamic trapping mechanism employed in the optimization is accurate and effective in immobilizing the microspheres. The framework is highly robust to consider different sizes of the microspheres in the optimization problem (Eqn. (8)). The other parameters in Eqn. (8) are also readily to modify with respect to varying requirements of device fabrication and applications.

This optimization framework also lays the foundation for future work to integrate lab-on-a-chip instrumentation, optical imaging, and statistical data analysis. The resulting integrated system should simplify image analysis, enable error-free target identification, and will be highly reliable, sensitive, and inexpensive.

4.3 Comparison with self assembled 3D microarrays

Here we discuss the comparison of our proposed microfluidic trap-based microsphere arrays with the current industrial 3D microarray standards, e.g., Illumina's BeadArray systems,.[6] First, the microspheres in Illumina's devices are randomly ordered and require several complex steps of hybridization and dehybridization to identify their types. Our device can combine micromechanical valves and isolated microfluidic chambers to trap different types of microspheres at predetermined locations (position encoding), and use the locations to identify the types.[20,21] This position encoding feature makes the target identification simple and error-free. Second, Illumina's devices can identify thousands of different microspheres and thus can be applied to genotyping and gene expression profiling. However, due to the requirement of chambers, our device applies only when the number of microspheres types (i.e., target types) is small or moderate, which is a limitation of our device. Finally, the microspheres in Illumina's devices are permanently immobilized and thus the captured targets cannot be recovered. In contrast, the microspheres are not permanently immobilized in our device. Therefore, our device can recover minute and precious captured targets after imaging, for subsequent studies or assays.

5. CONCLUSIONS

In this work, we proposed a novel microfluidic trap-based microsphere array device and employed fluidic resistance to hydrodynamically trap the microspheres. We built a comprehensive, robust, but simple framework to optimize the geometry of the trap arrays to maximize the packing density, with simultaneous salification of other criteria, such as efficiently immobilizing the microspheres, avoiding channel clogging, and minimizing the error in subsequent imaging experiments. Microsphere-trapping experiments confirmed that the optimized device significantly outperformed the un-optimized device, with respect to the optimization goal and criteria.

In future work, we will combine the optimized device with statistically designed position-encoded microsphere arrays.[20,21] We will further extend our optimization framework to develop a device for simultaneously detecting targets of diverse types, and thus achieve a multifunctional platform.

ACKNOWLEDGMENTS

This work was supported by the National Science Foundation Grant CIF:IHCS-0963742.

REFERENCES

[1] Oosterbroek, R. E., and Van den Berg, A., [Lab-on-a-chip: miniaturized systems for (bio)chemical analysis and synthesis], Elsevier B.V., Amsterdam (2003).

[2] Srinivasan, V., Pamula, V. K., and Fair, R. B., "An integrated digital microfluidic lab-on-a-chip for clinical diagnostics on human physiological fluids," Lab Chip, 4(4), 310-315 (2004).

[3] Cheng, I.-F., Chang, H.-C., Hou, D., and Chang, H.-C., "An integrated dielectrophoretic chip for continuous bioparticle filtering, focusing, sorting, trapping, and detecting," Biomicrofluidics, 1, 021503 (2007).

[4] Bontoux, N., Dauphinot, L., Vitalis, T., Studer, V., Chen, Y., Rossier, J., and Potier, M.-C., "Integrating whole transcriptome assays on a lab-on-a-chip for single cell gene profiling," Lab Chip, 8(3), 443-450 (2008).

[5] Fodor, S. P. A., Read, J. L., Pirrung, M. C., Stryer, L., Lu, A. T., and Dennis, S., "Light-directed, spatially addressable parallel chemical synthesis," Science, 251(4995), 767-773 (1991).

[6] Gunderson, K. L., Kruglyak, S., Graige, M. S., Wickham, E., Bierle, J., Doucet, D., Milewski, M., Yang, R., Siegmund, C., Haas, J., Zhou, L., and Chee, M. S., "Decoding randomly ordered DNA arrays," Genome Res., 14(5), 870-877 (2004).

[7] Situma, C., Hashimoto, M., and Soper, S. A., "Merging microfluidics with microarray-based bioassays," Biomol. Eng., 23(5), 213-231 (2006).

[8] Tan, W. H., and Takeuchi, S., "A trap-and-release integrated microfluidic system for dynamic microarray applications," Proc. Natl. Acad. Sci. USA, 104(4), 1146-1151 (2007).

[9] Sarder, P., and Nehorai, A., "Statistical design of position-encoded microsphere arrays," IEEE Trans. NanoBiosci., 10(1), 16-29 (2011).

[10] Wyss, H. M., Blair, D. L., Morris, J. F., Stone, H. A., and Weitz, D. A., "Mechanism for clogging of microchannels," Phys. Rev. E, 74, 061402 (2006).

[11] Kirby, B. J., [Micro- and Nanoscale Fluid Mechanics: Transport in Microfluidic Devices], Cambridge University Press, Cambridge, Chapter 3 (2010).

[12] Bruus, H., [Theoretical microfluidics], Oxford University Press, Oxford, Chapter 2 (2008).

[13] McDonald, J. C., and Whitesides, G. M., "Poly(dimethylsiloxane) as a material for fabricating microfluidic devices," Acc. Chem. Res. 35(7), 491-499 (2002).

[14] White, F. M., [Fluid mechanics], McGraw-Hill, New York, (2002).

[15] Manning, F. S., and Thompson, R. E., [Natural Gas], PennWell Books, Tulsa, (1991).

[16] Campbell, S. A., [The Science and Engineering of Microelectronic Fabrication], Oxford University Press, Oxford, Chapter 7 (2011).

[17] Dantzig, G. B., and Thapa, M. N., [Linear programming 2: theory and extensions], Springer-Verlag, New York, (2003).

[18] Kolda, T. G., Lewis, R. M., and Virginia, T., "Optimization by direct search: new perspectives on some classical and modern methods," SIAM Rev., 45(3), 385-482 (2003).

[19] Li, Z., and Demetri, P., "Optofluidic distributed feedback dye lasers," IEEE J. Sel. Top. Quant. Electron., 13(2), 185-193 (2007).

[20] Xu, X., Sarder, P., and Nehorai, A., "Statistical design of position-encoded microsphere arrays at low target concentrations," Proc. 45th Asilomar Conf. Signals, Syst. Comput., 1694-1698 (2011).

[21] Xu, X., Sarder, P., Kotagiri, N., Achilefu, S., and Nehorai, A., "Performance analysis and design of position-encoded microsphere arrays using the Ziv-Zakai bound," to appear in IEEE Trans. on NanoBiosci.